Sixth International Symposium on Turbulence and Shear Flow Phenomena
Seoul, Korea, 22-24 June 2009

DIRECT NUMERICAL SIMULATION OF TURBULENT FLOW IN AN AXISYMMETRIC SUPERSONIC DIFFUSER

Somnath Ghosh and **Rainer Friedrich**
Lehrstuhl für Aerodynamik,
Technische Universität München,
D-85748 Garching, Germany

ABSTRACT

Effects of deceleration and mean dilatation on the turbulence structure of supersonic flow in a diffuser with an incoming supersonic fully-developed turbulent pipe flow are studied by means of DNS. Strong enhancement of the turbulence intensities is observed when the flow undergoes deceleration. Turbulence production and pressure-strain terms in the Reynolds stress budgets are found to increase dramatically leading to increased Reynolds stresses. The central role of pressure-strain correlations in modifying the turbulence structure in these flow conditions is demonstrated.

INTRODUCTION

Decelerated compressible wall-bounded turbulent shear flows are still of great practical and theoretical interest and provide a challenge for improved turbulence modeling. Incompressible adverse pressure gradient (APG) shear flows have been studied experimentally among others by Nagano *et al.* (1997) and numerically by Coleman *et al.* (2003) and Lee & Sung (2008). When the flow is compressible and undergoes an APG, the turbulence structure is affected not only by mean strain and shear, but also by mean compression. In his pioneering work, Bradshaw (1974) studied effects of mean dilatation on the turbulence structure in wall-bounded flows in the context of engineering calculation methods. He found that mean dilatation effects have a greater impact on the turbulence structure than would be expected from the extra production terms in the Reynolds stress transport equations. He also mentioned indirect effects caused by the pressure-strain correlation tensor in such flows which can add 'overwhelmingly' to those of the extra production terms. In their experimental investigation of APG supersonic turbulent boundary layers, Fernando & Smits (1990) studied the behaviour of the Reynolds stresses and of the large-scale structures. Recently, Ghosh *et al.* (2008) performed DNS/LES of supersonic axisymmetric nozzle flow and also LES of supersonic diffuser flow using a fully-developed pipe flow at the inlet in order to study, among other features, Bradshaw's indirect effect of the pressure-strain correlations on the turbulence structure. They found that the Reynolds stresses and pressure-strain correlations are dramatically increased in the diffuser even though the production by mean strain and mean compression is relatively small compared to that by mean shear. Now, supersonic internal flows subjected to APGs are more complicated than corresponding flows subjected to favourable pressure gradients (nozzle flow) so that their analysis needs greater care. When the Mach number of the incoming flow is at a rather low overall supersonic level and the flow contraction is moderate, substantial transonic regions can occur. It is the aim of this paper to gain insight into the complex dynamics of a supersonic diffuser flow which develops from an incoming fully-developed pipe flow. The results will provide a data-base for validation and improvement of Reynolds stress models. Apriori-tests of two existing pressure-strain models are carried out using DNS data.

NUMERICAL DETAILS

The governing Navier-Stokes equations are solved in a characteristic-type pressure-velocity-entropy form on non-orthogonal curvilinear coordinates. Fifth order compact upwind schemes with low dissipation (Adams & Shariff, 1996) have been used for the convection terms and sixth order compact central schemes (Lele, 1992) for the molecular transport terms. The flow field is advanced in time using a 3rd order low-storage Runge-Kutta scheme (Williamson, 1980). Fully-developed supersonic turbulent flow in a pipe serves as inflow condition for the diffuser flow. The walls are kept at the same constant temperature in both the flows. The centerline Mach number M_c and friction Reynolds number Re_τ of the incoming flow are 1.75 and 300. Re_τ is defined using the friction velocity $u_\tau = \sqrt{\tau_w/\rho_w}$, the pipe radius R and the kinematic viscosity at the wall, $\nu_w(T_w)$. The Mach number M_c is the ratio of the centerline velocity and local speed of sound. The domain length of each configuration (pipe or diffuser) is $L = 10R$. The adverse axial pressure gradient averaged over the first half of the diffuser and normalized with the local displacement thickness and the local wall shear stress (Clauser parameter) is 5. The ratio of diffuser radius to pipe radius at the end of the computational domain is 0.93. The number of grid points used to discretize the pipe domain is $256 \times 256 \times 140$ in streamwise, circumferential and radial directions while that for the diffuser is $384 \times 256 \times 140$. The higher resolution in the diffuser is required to capture the increased turbulence activity occurring due to deceleration of the flow. The pipe and diffuser flow simulations are coupled using MPI routines. The concept of characteristics is applied to set inviscid inflow conditions for the diffuser flow. The incoming characteristics are computed from the periodic pipe flow simulations and are received at every time-step in the diffuser computation through MPI. Partially non-reflecting outflow conditions are used in the subsonic region of the outflow plane. No sponge layer has been used (Ghosh *et al.*, 2008).

RESULTS

Instantaneous and mean flow features

A snapshot of instantaneous axial velocity fluctuations, normalized with the local friction velocity, and presented in an (x, r)-plane that contains the axis, is shown in Figure 1. An increase in near-wall 'sweep-ejection' activity as the flow is decelerated, can be observed in the first half of this carpet

Sixth International Symposium on Turbulence and Shear Flow Phenomena
Seoul, Korea, 22-24 June 2009

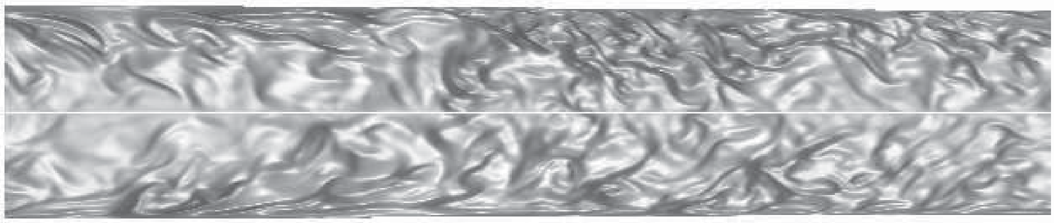

Fig. 1: Axial velocity fluctuations, normalized with local $\sqrt{\tau_w/\rho_w}$, in a (x,r)- plane of the diffuser. Amplitudes range from -15 to +15. Flow is from left to right.

plot. The carpet plot also shows the weak overall decrease in cross-sectional area. Since the Mach number of the incoming turbulent pipe flow is low supersonic ($M_c = 1.75$), substantial transonic regions appear after about 50% of the diffuser length, even though the contraction is weak. So, it is important to look at bulk, centerline and inner layer quantities in order to better understand the complex flow behaviour and demarcate regions of deceleration and acceleration. Figure 2 shows the axial development of the bulk values of Mach number, density, velocity, mass flux and Reynolds number. All bulk variables are obtained by averaging local mean variables over the circular cross-section and, except for the Mach number M_m, they are normalized by their inlet values. M_m drops from a value of 1.5 over 60% of the diffuser length and then shows a weak increase in the rest of the diffuser. The acceleration in the later part of the diffuser is caused by growth of the near-wall subsonic layer when the flow decelerates, and the continual reduction in cross-sectional area. The behaviour of the bulk velocity clearly indicates deceleration in the first half (and acceleration in the second), while the bulk density first increases and then decreases. The bulk Reynolds number which is based on the local diffuser radius shows a decrease in the first half and an increase in the second. Figure 3 presents mean values at the centerline. While the Mach number M_c drops, the pressure, density and temperature increase up to $x/L = 0.6$, underlining the effect of deceleration in a supersonic diffuser whose cross-section A decreases by roughly 4% in the first half. In Figure 4 we note in the first 40% of the diffuser length a decrease in the wall shear stress, the friction Mach number $M_\tau = u_\tau(x)/c_w$ and the friction Reynolds number $Re_\tau = u_\tau(x)\bar{\rho}_w(x)R(x)/\mu_w$ and an increase in the ratio of displacement to momentum thickness, H. For completeness we note the reference flow parameters: $Re_m(0) = 2766$, $Re_c(0) = 3857$, $M_\tau(0) = 0.087$, $Re_\tau(0) = 300$ and $H(0) = 2.0$.

In this paper, we are interested in looking at effects of deceleration on the turbulence structure. So, we restrict our analysis to the first half of the diffuser where the flow is clearly decelerated. The mean extra strain rate is limited to less than 15% of the mean shear in the peak production zone. A look at the local Mach number profiles (fig. 5) reveals the deceleration at $x/L = 0.2, 0.35$. These profiles also give an impression of the growth of the near-wall subsonic layer. Profiles at positions $x/L = 0.6, 0.95$ show the acceleration of the flow first in the subsonic layer ($x/L = 0.6$) and then across the entire cross-section ($x/L = 0.95$). In the remaining part of the paper, we will discuss profiles up to $x/L = 0.35$ only and analyse the effects of mean compression on the turbulence structure. The mean density and mean temperature continue to show a roughly inverse proportionality in the radial direction (fig. 6) as in the incoming pipe flow since the radial variation of mean pressure remains negligible. The mean temperature is increased both by increase in mean and turbulent dissipation. The Van Driest transformed mean velocity profiles (fig. 7) show an overshoot over the log law for pipe flows, in a manner similar to incompressible flows under the influence of APG. However, here the variation of density in the axial direction is also reflected in the Van Driest transformed profiles.

Effects of deceleration on the turbulence structure

Deceleration of the supersonic flow in the diffuser leads to an increase in turbulence intensities. As a result, both solenoidal and dilatational dissipation rates, $\bar{\rho}\epsilon_s = \bar{\mu}\overline{\omega_i'\omega_i'}$, $\bar{\rho}\epsilon_d = 4/3\bar{\mu}\overline{s_{kk}'s_{ll}'}$ are enhanced (figs. 8,9). An increase in pressure-dilatation correlation $\overline{p'u_{i,i}'}$ is also observed. However, compressible dissipation rate as well as pressure-dilatation correlation continue to have negligible contributions to the TKE budget as in the incoming supersonic pipe flow. The increase in solenoidal dissipation rate can be explained intuitively from its transport equation (Kreuzinger *et al.*, 2006) in which a production term appears that contains mean dilatation. The Reynolds stresses increase monotonously through the compression region, both in the near-wall region as well as in the core. Here we show the axial Reynolds stress and the Reynolds shear stress scaled with the local wall shear stress (figs. 10,11). The rms axial and radial intensities scaled with constant friction velocity, $u_{\tau,o}$ of the incoming flow (figs. 12,13) reveal the same trend, but in this scaling the magnitude of the enhancement is reduced. It should be noted that while in incompressible boundary layers under the influence of APG, the turbulence intensities are decreased in the near-wall region and increased in the outer layer (Lee & Sung, 2008), in the compressible diffuser flow, we see an increase in turbulence intensities both near the wall as well as in the core region.

The axial Reynolds stress production is increased and the production term is now decomposed into contributions from mean shear, extra strain rate and mean compression as in eq.(1). Extra strain rate and mean compression lead to small increases in the production of the axial stress as seen in fig. 14. But, the major increase in production is due to production by mean shear. The mean shear itself changes only marginally in the peak production region (as shown in fig. 11 at $x/L = 0.2$ and 0.35) which means that the increase in the Reynolds shear stress is the main reason for the increase in production by mean shear. This is contrary to findings in incompressible decelerated channel flows (Coleman *et al.*, 2003) where decreased mean shear leads to decreased production (and hence decreased turbulence intensities) in the near-wall region. The production term in the shear stress equation is similarly decomposed (eq. 2) and again production due to mean shear (*shear1*) is the main reason for an increase in Reynolds shear stress (fig. 15). The term *shear2* has a small negative contribution, while production by mean dilatation and extra rate of strain remain equally small. The remarkable increase in production by mean shear is caused

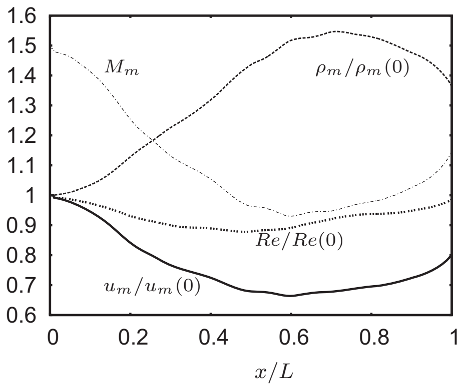

Fig. 2: Bulk quantities.

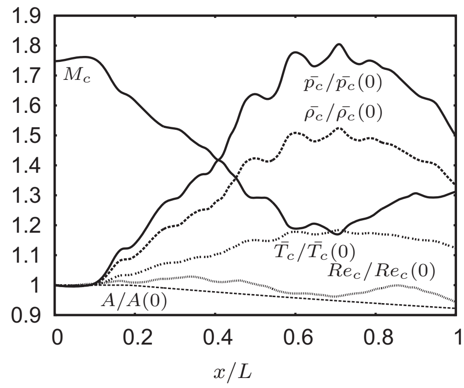

Fig. 3: Centerline quantities.

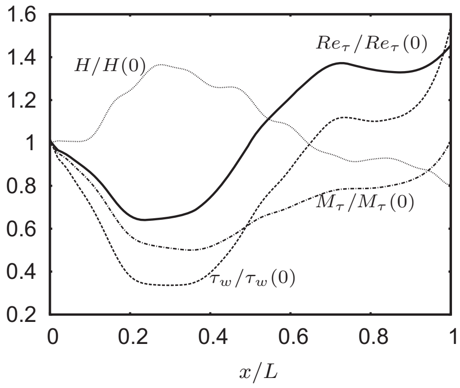

Fig. 4: Inner layer quantities.

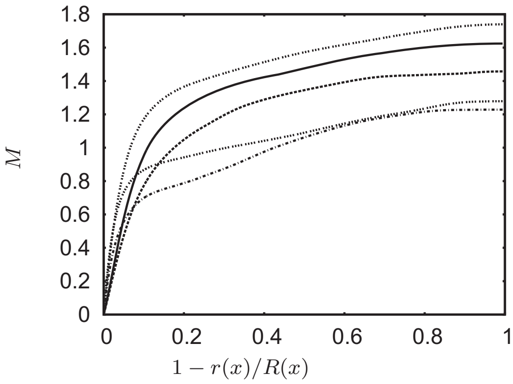

Fig. 5: Local mean Mach number. $x/L = 0$ (... ...), 0.2(—), 0.35(− − −), 0.6(−. − .−), 0.95(.... ....)

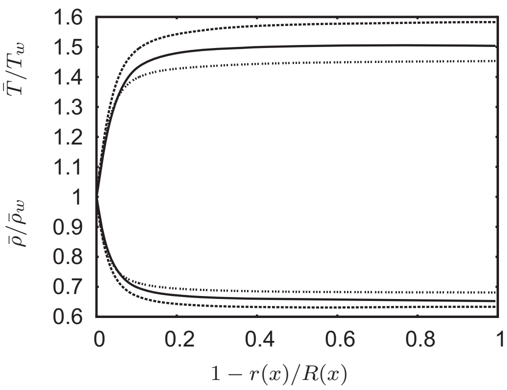

Fig. 6: Mean density, temperature $x/L = 0$(... ...), 0.2(—), 0.35(− − −)

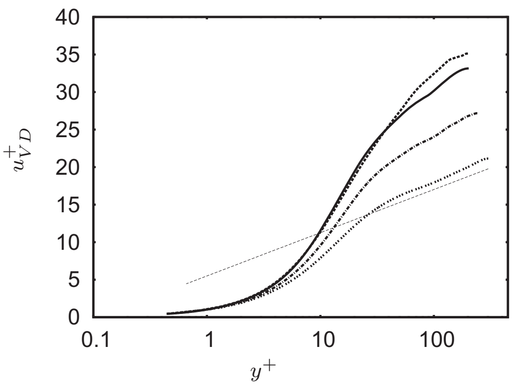

Fig. 7: Van Driest transformed velocity $x/L = 0$(... ...), 0.15(−. − .−), 0.2(—), 0.35(− − −)
Straight line: $u^+ = 2.5lny^+ + 5.5$

by increased radial stress, which in turn increases due to the dramatic increase in the redistributive pressure-strain correlations (figs.16, 17). Thus the pressure-strain correlations play a significant role in controlling turbulence production in this flow. Both pressure fluctuations and strain rate fluctuations are found to increase.

$$P_{xx} = \underbrace{-\overline{\rho u_x'' u_r''}\frac{\partial \widetilde{u_x}}{\partial r}}_{shear} \underbrace{-\frac{1}{3}\overline{\rho u_x'' u_x''}\frac{\partial \widetilde{u_l}}{\partial x_l}}_{mean\ dilatation} \underbrace{-\overline{\rho u_x'' u_x''}(\frac{\partial \widetilde{u_x}}{\partial x} - \frac{1}{3}\frac{\partial \widetilde{u_l}}{\partial x_l})}_{extra\ rate\ of\ strain} \quad (1)$$

$$P_{xr} = \underbrace{-\overline{\rho u_r'' u_r''}\frac{\partial \widetilde{u_x}}{\partial r}}_{shear1} \underbrace{-\overline{\rho u_x'' u_x''}\frac{\partial \widetilde{u_r}}{\partial x}}_{shear2} \underbrace{-\frac{2}{3}\overline{\rho u_x'' u_r''}\frac{\partial \widetilde{u_l}}{\partial x_l}}_{mean\ dilatation} \underbrace{-\overline{\rho u_x'' u_r''}(\frac{\partial \widetilde{u_x}}{\partial x} + \frac{\partial \widetilde{u_r}}{\partial r} - \frac{2}{3}\frac{\partial \widetilde{u_l}}{\partial x_l})}_{extra\ rate\ of\ strain} \quad (2)$$

Apriori-test of pressure strain models

The pressure-strain correlation can be written as the sum of a 'slow' part proportional to the local turbulence anisotropy and a 'rapid' part proportional to mean strain rates. Lai & So (1990) applied a near-wall extension of the

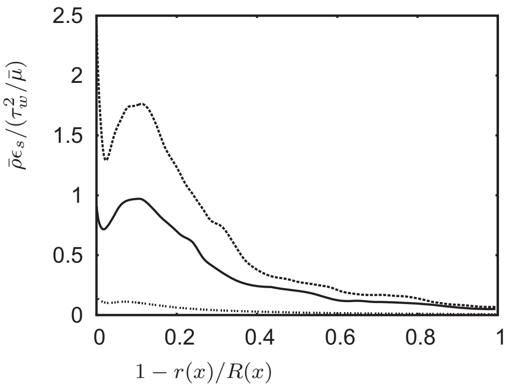

Fig. 8: Solenoidal dissipation.
Line types as in fig. 6

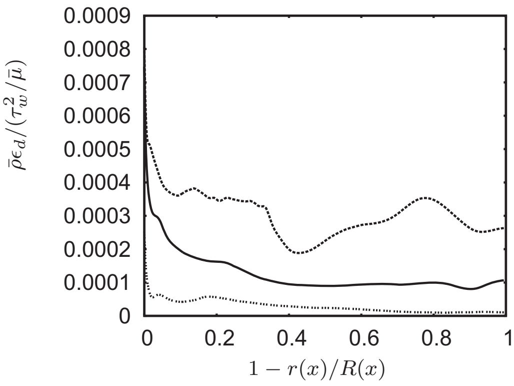

Fig. 9: Dilatational dissipation
Line types as in fig. 6

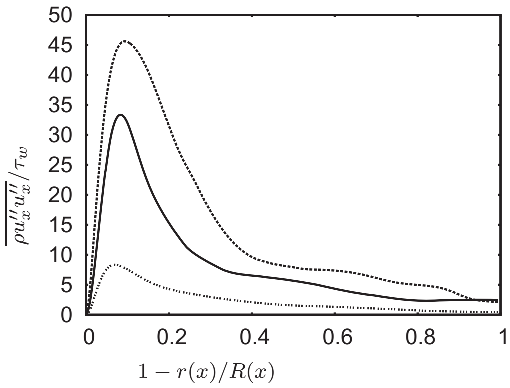

Fig. 10: Axial Reynolds stress.
Line types as in fig. 6

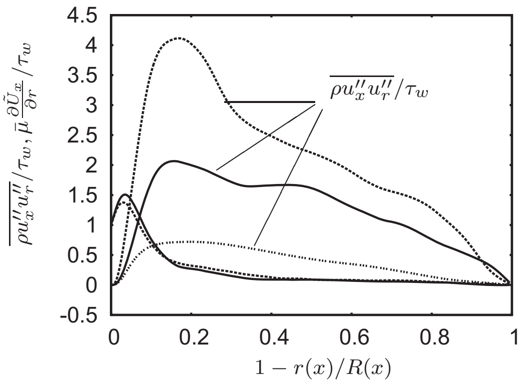

Fig. 11: Reynolds shear stress, mean shear
Line types as in fig. 6

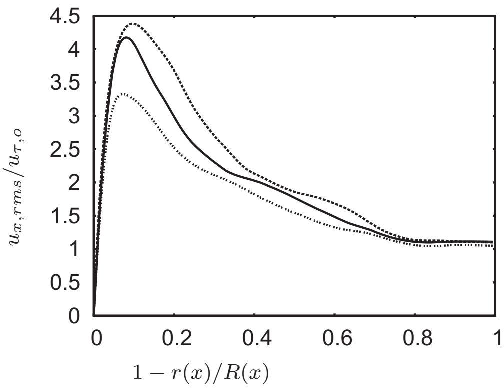

Fig. 12: Axial rms intensity.
Line types as in fig. 6

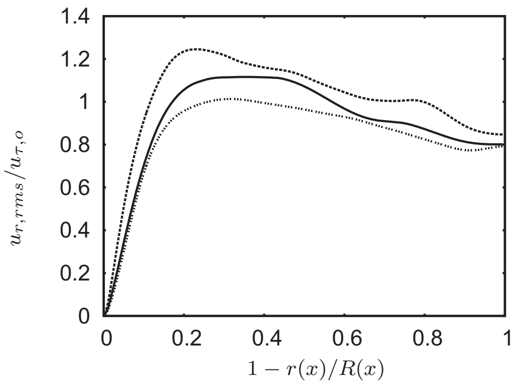

Fig. 13: Radial rms intensity
Line types as in fig. 6

LRR model (Launder *et al.*, 1975) to incompressible pipe flows and found reasonable agreement with DNS data. So *et al.* (1998) derived a near-wall, variable density extension of the SSG model (Speziale *et al.*, 1991) using Morkovin's hypothesis and applied this to supersonic boundary layers. In this paper, we use near-wall variable density extensions of both these models to predict the axial pressure-strain correlations using DNS data. The objective is not only to see how these models perform in this complex flow, but also to look at the behaviour of the rapid and slow parts of the pressure-strain correlations.

Following So *et al.* (1998), the pressure-strain correlations are expressed as

$$(\overline{p'u'_{i,j}} + \overline{p'u'_{j,i}}) = \bar{\rho}(\Phi_{ij} + \Phi_{ij}^w) \quad (3)$$

For ease of notation, we use Cartesian coordinates. The near-wall LRR model for Φ_{ij}, Φ_{ij}^w as in Lai & So (1990) are:

$$\Phi_{ij} = -2C_1\epsilon_s b_{ij} - \alpha(P_{ij} - \frac{2}{3}\delta_{ij}\tilde{P}) - \beta(D_{ij} - \frac{2}{3}\delta_{ij}\tilde{P}) - 2\gamma k S_{ij} \quad (4)$$

$$\Phi_{ij}^w = f_w[2C_1\epsilon_s b_{ij} - \frac{\epsilon_s}{k}(\widetilde{u_i u_k} n_k n_j) + \alpha^*(P_{ij} - \frac{2}{3}\delta_{ij}\tilde{P})] \quad (5)$$

The near-wall SSG model for Φ_{ij}, Φ_{ij}^w as in So *et al.*

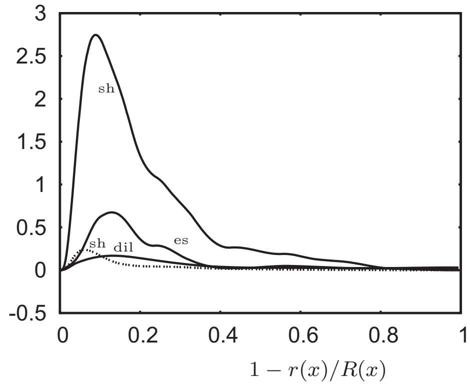

Fig. 14: Decompostion of axial stress production at $x/L = 0(\ldots\ \ldots)$ and 0.35 (—)

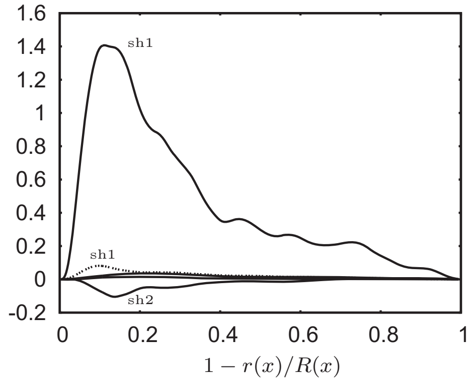

Fig. 15: Decomposition of shear stress production at $x/L = 0$ (... ...) and 0.35 (—)

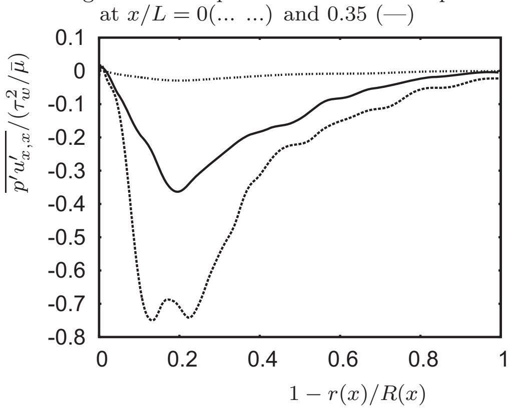

Fig. 16: Axial pressure-strain correlations (Π_{xx}). Line types as in fig. 6

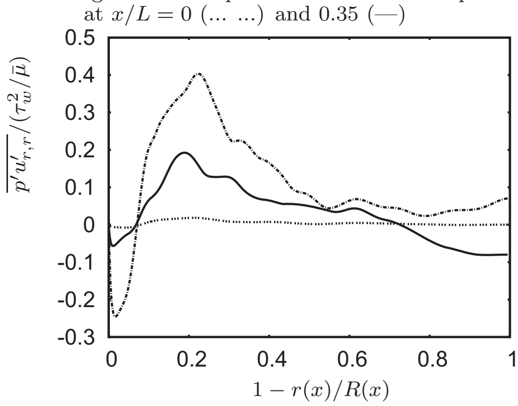

Fig. 17: Radial pressure-strain correlations Line types as in fig. 6

(1998) are :

$$\Phi_{ij} = -(2C_1\epsilon_s + C_1^*\tilde{P})b_{ij} + C_2\epsilon_s(b_{ik}b_{kj} - \frac{1}{3}\Pi\delta_{ij}) - \alpha(P_{ij} - \frac{2}{3}\delta_{ij}\tilde{P}) - \beta(D_{ij} - \frac{2}{3}\delta_{ij}\tilde{P}) - 2[\gamma + (C_3^*/2)\Pi^{0.5}]kS_{ij} \quad (6)$$

$$\Phi_{ij}^w = f_w[(2C_1\epsilon_s + C_1^*\tilde{P})b_{ij} - C_2\epsilon_s(b_{ik}b_{kj} - \frac{1}{3}\Pi\delta_{ij}) + \alpha^*(P_{ij} - \frac{2}{3}\delta_{ij}\tilde{P}) + 2\gamma_{ij}^*] + \Pi_{ij}^p \quad (7)$$

where $\epsilon_s = \bar{\nu}\overline{\omega_i'\omega_i'}$, $b_{ij} = (\widetilde{u_i''u_j''} - 2k\delta_{ij}/3)/2k$, $S_{ij} = (\tilde{U}_{i,j} + \tilde{U}_{j,i})/2$, $P_{ij} = -(\widetilde{u_i''u_k''}\tilde{U}_{j,k} + \widetilde{u_j''u_k''}\tilde{U}_{i,k})$, $\tilde{P} = P_{ii}/2$ $D_{ij} = -(\widetilde{u_i''u_k''}\tilde{U}_{k,j} + \widetilde{u_j''u_k''}\tilde{U}_{k,i})$, $\Pi = b_{ij}b_{ij}$

The constants used are the same as given in Lai & So (1990), So *et al.* (1998). The wall function f_w is given by $f_w = exp(-(ARe_t/60)^3)$ as explained in So *et al.* (1994).

The axial pressure-strain correlations (Π_{xx}) given by the LRR and SSG models (eqs. 3 -7) are evaluated using DNS data at two axial locations along the diffuser and compared with Π_{xx} obtained from the DNS in figs. 16 and 17. Substantial divergence from the DNS data in the near-wall region is observed although beyond a certain distance from the wall, $1 - r/R = 0.3$, there is some sort of collapse. At $x/L = 0.2$, both models underpredict the peak in Π_{xx} at $1 - r/R = 0.2$ and show non-physical peaks closer to the wall. At $x/L = 0.35$, the predictions of both the models are closer to the DNS data. A slight over-prediction by the SSG model and a marginal under-prediction by the LRR model are observed.

Both the rapid and slow parts of the models show large, monotonous increases as the flow is decelerated (figs. 18,19). From a modelling point of view, correct prediction of this increase is a challenging task because in this flow, the distortion is not really rapid, so that not only the rapid part, but also the slow part of the pressure-strain correlations needs to be considered.

CONCLUSIONS

Effects of a weak adverse pressure gradient on the turbulence structure of supersonic flow in a diffuser with incoming supersonic fully-developed pipe flow is investigated by means of DNS. Large increases in turbulence intensities occur when the flow undergoes deceleration. Turbulence production and pressure-strain correlations are increased. Analysis of the production terms shows that although the extra strain rate and mean compression increase turbulence production, their role is small compared to that of the redistributive pressure-strain correlations whose increase leads to a major increase in turbulence production by mean shear. Both pressure and strain rate fluctuations increase and further analysis is currently being performed to explain this.

Apriori tests of near-wall, variable-density extensions of LRR and SSG models for the axial pressure-strain correlations using DNS data reveal large modifications in both the rapid and slow parts of the models. The prediction of the axial pressure-strain correlations by both the models is found to be reasonable in the core region of the diffuser but needs to be improved in the near-wall region.

Sixth International Symposium on Turbulence and Shear Flow Phenomena
Seoul, Korea, 22-24 June 2009

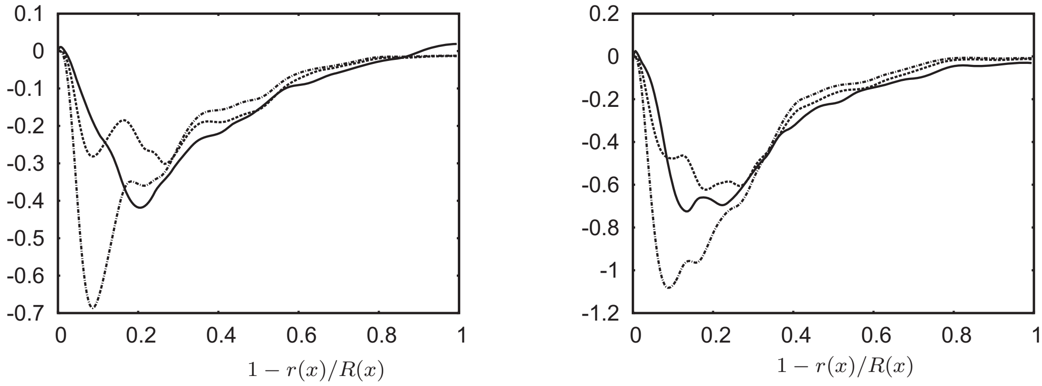

Figs. 18, 19: Π_{xx} in the diffuser at $x/L = 0.2$ (left) and $x/L = 0.35$ (right).
—, DNS, $- - -$, LRR, $-. - .-$, SSG

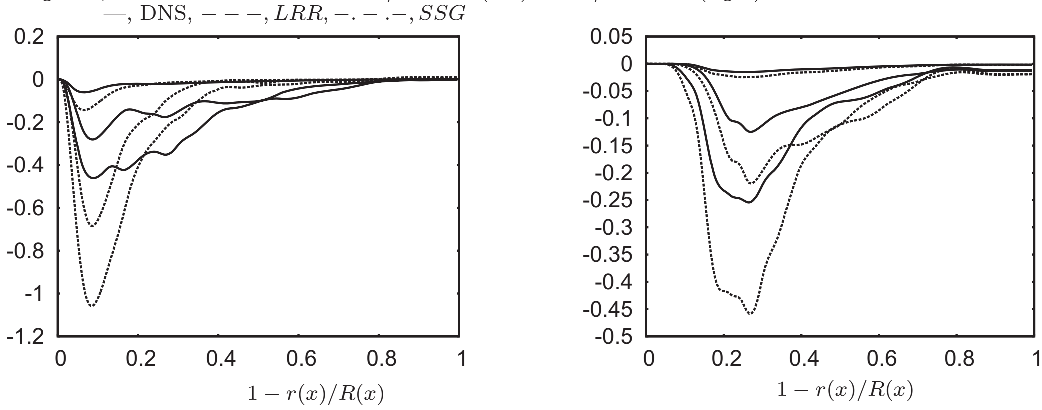

Figs. 20, 21: Rapid (left) and slow (right) parts of Π_{xx} in the diffuser. —,LRR, $- - -$, SSG.
$x/L = 0.1, 0.2, 0.35$ from top to bottom of fig.

*

References

Adams, N. A. & Shariff, K. 1996 A high-resolution hybrid compact-ENO scheme for shock-turbulence interaction problems. *Journal of Computational Physics* **127**, 27–51.

Bradshaw, P. 1974 The effect of mean compression or dilatation on the turbulence structure of supersonic boundary layers. *Journal of Fluid Mechanics* **63**, 449–464.

Coleman, G. N., Kim, J. & Spalart, P. R. 2003 Direct numerical simulation of a decelerated wall-bounded turbulent shear flow. *Journal of Fluid Mechanics* **495**, 1–18.

Fernando, E. M. & Smits, A. J. 1990 A supersonic turbulent boundary layer in an adverse pressure gradient. *Journal of Fluid Mechanics* **211**, 285–307.

Ghosh, S., Sesterhenn, J. & Friedrich, R. 2008 Large-eddy simulation of supersonic turbulent flow in axisymmetric nozzles and diffusers. *International J. of Heat and Fluid Flow* **29**, 579–590.

Kreuzinger, J., Friedrich, R. & Gatski, T. B. 2006 Compressibility effects in the solenoidal dissipation rate equation: A priori assessment and modeling. *International J. of Heat and Fluid Flow* **27**, 696–706.

Lai, Y.G & So, R.M.C 1990 On near-wall turbulent flow modelling. *Journal of Fluid Mechanics* **221**, 641–674.

Launder, B.E., Reece, G.J. & Rodi, W. 1975 Progress in the development of a Reynolds-stress turbulence closure. *Journal of Fluid Mechanics* **68**, 537–566.

Lee, J. & Sung, H. J. 2008 Effects of an adverse pressure gradient on a turbulent boundary layer. *International J. of Heat and Fluid Flow* **29**, 568–578.

Lele, S.K. 1992 Compact finite difference schemes with spectral-like resolution. *Journal of Computational Physics* **103**, 16–42.

Nagano, Y., Tsuji, T. & Houra, T. 1997 Structure of turbulent boundary layer subjected to adverse pressure gradient. *Eleventh Symp. on Turbulent Sear Flows, Grenoble, France, September 8-10* .

So, R.M.C., Aksoy, H., Sommer, T.P. & Yuan, S.P. 1994 Development of a near-wall Reynolds-stress closure based on the SSG model for the pressure-strain. *Tech. Rep.*. NASA CR-4618.

So, R. M. C, Gatski, T. B. & Sommer, T. P. 1998 Morkovin hypothesis and the modelling of wall-bounded compressible turbulent flows. *AIAA journal* **36** (9), 1583–1592.

Speziale, C. G., Sarkar, S. & Gatski, T. B. 1991 Modelling the pressure-strain correlation of turbulence: An invariant dynamical systems approach. *Journal of Fluid Mechanics* **227**, 245–272.

Williamson, J. K. 1980 Low-storage Runge-Kutta schemes. *Journal of Computational Physics* **35**, 48–56.